Inorganic Chemistry

including bioinorganic chemistry

May 19, 2014
Volume 53, Number 10
pubs.acs.org/IC

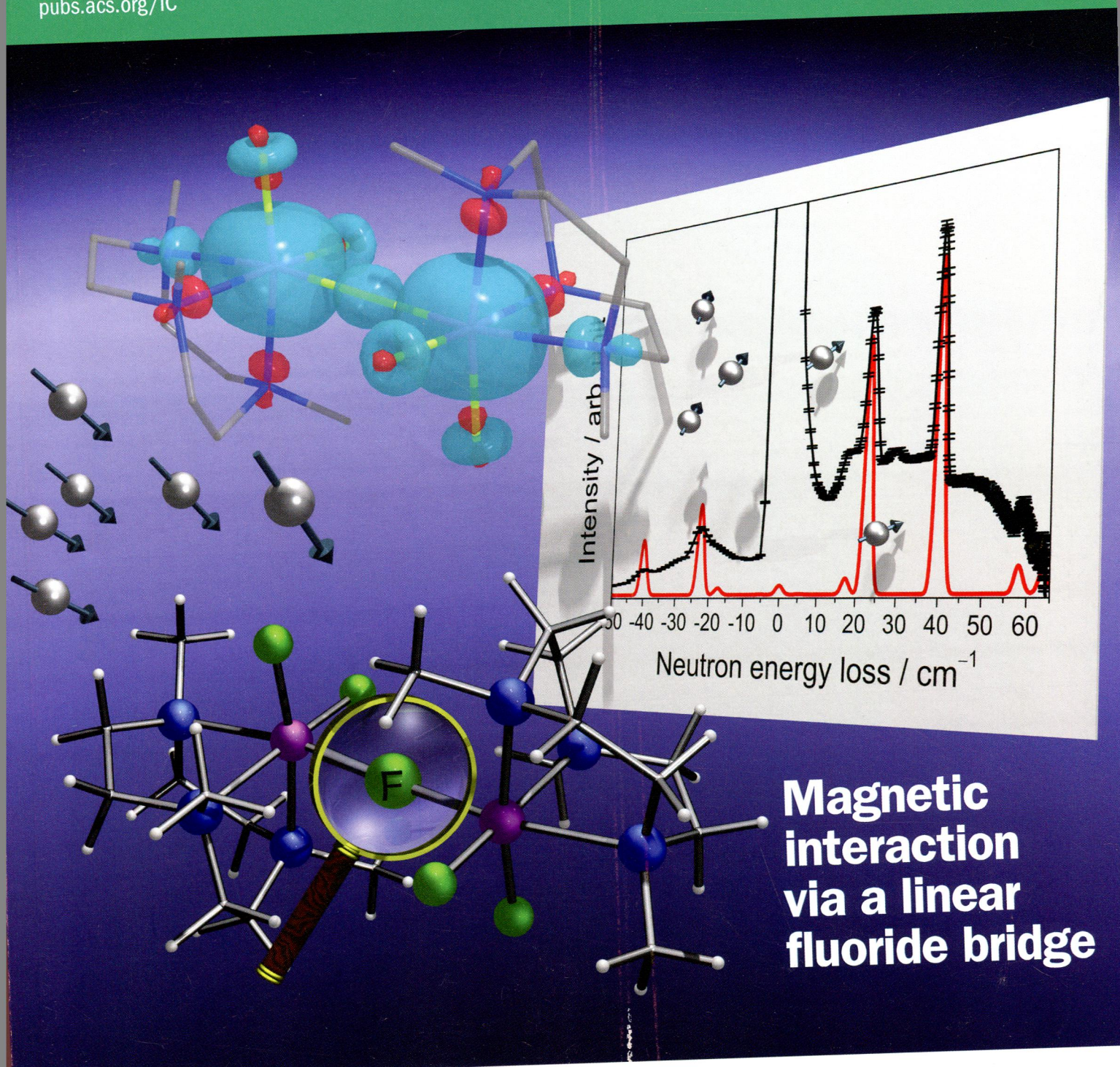

Magnetic interaction via a linear fluoride bridge

ACS Publications
Most Trusted. Most Cited. Most Read.

www.acs.org

Inorganic Chemistry

MAY 19, 2014
VOLUME 53 ISSUE 10

INOCAJ 53(10) 4791−5404 (2014)
ISSN 0020-1669
Registered in the U.S. Patent and Trademark Office

ON THE COVER: The magnetic interaction via a perfectly linear fluoride bridge in a simple, dinuclear manganese(III) complex is studied in detail by a range of techniques including inelastic neutron scattering, HF-EPR, and computational modeling. See K. S. Pedersen, M. Sigrist, H. Weihe, A. D. Bond, C. Aa. Thuesen, K. P. Simonsen, T. Birk, H. Mutka, A.-L. Barra, and J. Bendix, p 5013.

Communications

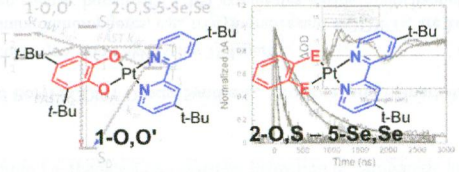

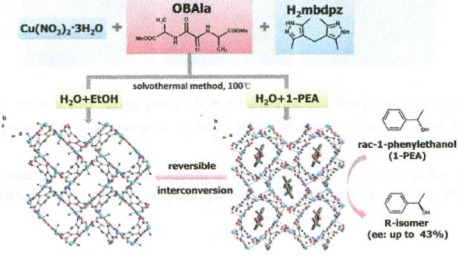

4797 S

dx.doi.org/10.1021/ic500531k

Metalloporphyrinic Framework Containing Multiple Pores for Highly Efficient and Selective Epoxidation

Xiu-Li Yang and Chuan-De Wu*

The connection between paddle-wheel $Zn_2(COO)_4$ building units and metalloporphyrins having eight carboxylate groups results in an interesting porous porphyrinic framework that contains multiple pores and demonstrates high efficiency and stability upon epoxidation of olefins with excellent substrate size selectivity.

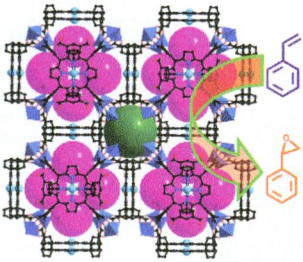

4800 S

dx.doi.org/10.1021/ic500744s

Variation of the Eu^{II} Emission Wavelength by Substitution of Fluoride by Hydride in Fluorite-Type Compounds EuH_xF_{2-x} ($0.20 \leq x \leq 0.67$)

Nathalie Kunkel,* Andries Meijerink, and Holger Kohlmann*

Eu^{2+} luminescence in mixed-hydride fluorides is observed for the first time. In EuH_xF_{2-x} ($0.20 \leq x \leq 0.67$), the energy of the emission depends strongly on the degree of substitution x. The red shift for higher hydride contents is attributed to the nephelauxetic effect of the hydride anion. The strong x dependence of the luminescence maxima proves the hydride–fluoride substitution to be a valuable tool to tune the emission wavelength of Eu^{II}-containing phosphors.

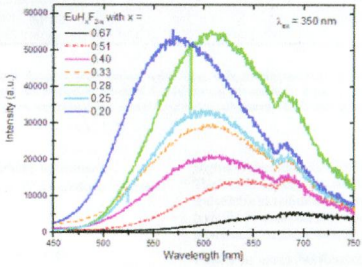

Articles

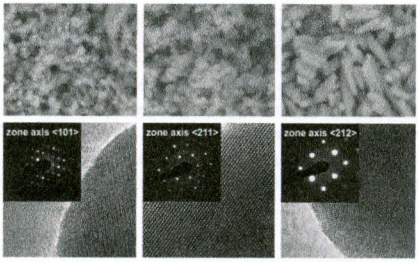

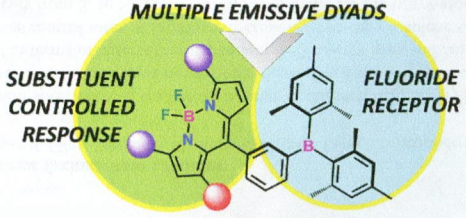

4824 S dx.doi.org/10.1021/ic402650g

Syntheses and Molecular Structures of Monomeric and Hydrogen-Bonded Dimeric Dawson-Type Trialuminum-Substituted Polyoxotungstates Derived under Acidic and Basic Conditions

Chika Nozaki Kato,* Toshifumi Kashiwagi, Wataru Unno, Miyuki Nakagawa, and Hidemitsu Uno

The syntheses and molecular structures of the two types of α-Dawson-type trialuminum-substituted polyoxometalates, $[B\text{-}\alpha\text{-}H_3P_2W_{15}O_{59}\{Al(OH_2)\}_3]^{6-}$ (**1**) and $[B\text{-}\alpha\text{-}H_3P_2W_{15}O_{59}\{Al(OH)\}_2\{Al(OH_2)\}]_2^{16-}$ (**2**), are described herein. The polyoxoanion **1** is a monomeric, α-Dawson-type structure, resulting in an overall C_{3v} symmetry, while the polyoxoanion **2** is a hydrogen-bonded dimeric structure, resulting in an overall S_3 symmetry in the solid state.

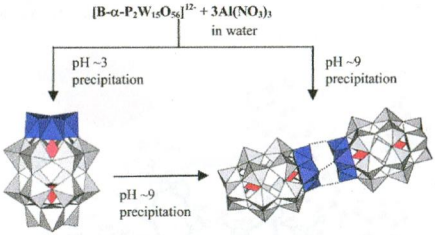

4833 S dx.doi.org/10.1021/ic402653f

Electronic Structure of Low-Dimensional $4d^5$ Oxides: Interplay of Ligand Distortions, Overall Lattice Anisotropy, and Spin–Orbit Interactions

Vamshi M. Katukuri, Karla Roszeitis, Viktor Yushankhai, Alexander Mitrushchenkov, Hermann Stoll, Michel van Veenendaal, Peter Fulde, Jeroen van den Brink, and Liviu Hozoi*

The splitting of transition-metal t_{2g} and e_g levels in noncubic environments is usually associated with distortions of the first ligand coordination shell. We here show that the anisotropy of the farther surroundings may have a stronger effect and give rise to, e.g., negative tetragonal splittings even in the presence of positive tetragonal distortions of the NN ligands. The effect of longer-range anisotropy is expected to be stronger in 4d and 5d systems because the more extended 4d and 5d functions feel more effectively how the anisotropic crystalline fields vary along different directions in space. The different 4d (5d) components are, however, admixed because of strong spin–orbit couplings, and this makes interpretation of the experimental spectra difficult. Ab initio many-body calculations are in this context of great use.

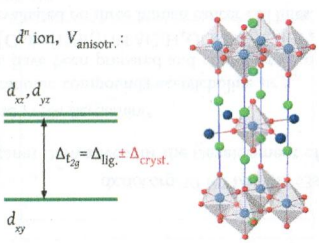

4840 S dx.doi.org/10.1021/ic402649b

White Phosphorus Degradation with a NacNac Aluminum Carbene Analogue: The Biradical Reaction Mechanism

Wolfgang W. Schoeller* and Guido D. Frey

The AlNacNac compound adds to white phosphorus over a biradical mechanism to the formal double-insertion product.

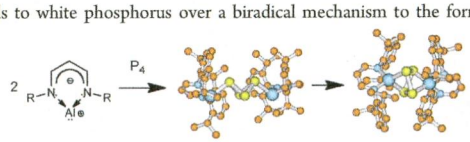

4847 S dx.doi.org/10.1021/ic4028157

Stereochemical Diversity of {MNO}^{10} Complexes: Molecular Orbital Analyses of Nickel and Copper Nitrosyls

Jeanet Conradie and Abhik Ghosh*

Metal–NO bonding in the $[Cu(CH_3NO_2)_5(NO)]^{2+}$ cation, a $\{CuNO\}^{10}$ complex, consists of a single $Cu(d_{z^2})$–$NO(\pi^*)$ σ-interaction and essentially no $metal(d_\pi)$–$NO(\pi^*)$ π-bonding, explaining both the bent CuNO geometry and the long, weak Cu–N(O) bond.

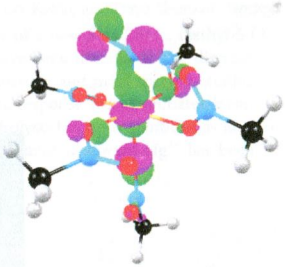

4856 S dx.doi.org/10.1021/ic402864s

Mild Solvothermal Syntheses and Characterization of Layered Copper Thioantimonates(III) and Thioarsenate(III)

Chi Zhang, Min Ji, Shou-Hua Ji, and Yong-Lin An*

Solvothermal syntheses of inorganic layered copper thioantimates(III) $A_2Cu_2Sb_2S_5$ (A = Rb, Cs) and copper thioarsenate(III) $Rb_8Cu_6As_8S_{19}$ have been carried out under mild conditions.

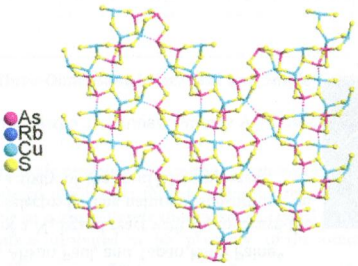

4861 S dx.doi.org/10.1021/ic402936z

Preparation of *N,N*-Dialkylcarbamato Lanthanide Complexes by Extraction of Lanthanide Ions from Aqueous Solution into Hydrocarbons

Lidia Armelao, Daniela Belli Dell'Amico,* Paolo Biagini, Gregorio Bottaro, Stefano Chiaberge, Paola Falvo, Luca Labella, Fabio Marchetti, and Simona Samaritani

Lanthanides are easily extracted as *N,N*-dibutylcarbamato complexes from aqueous solutions into heptane containing dibutylamine saturated with CO_2. The products are recovered in high yields. The derivatives $[Ln(O_2CNBu_2)_3]_n$ (Ln = Nd, Eu, Tb), $[NH_2Bu_2]_2[Ln_4(CO_3)(O_2CNBu_2)_{12}]$ (Ln = Eu, Sm, Tb), and $[Sm_4(CO_3)(O_2CNBu_2)_{10}]$ have thus been obtained. The crystal and molecular structure of $[NH_2Bu_2]_2[Tb_4(CO_3)(O_2CNBu_2)_{12}]$ has been solved, with the analogous samarium and europium complexes being iso-structural. Mass spectra and photoluminescence studies have been carried out.

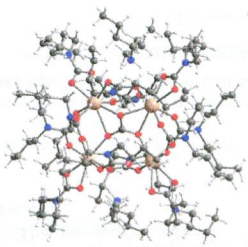

4872 dx.doi.org/10.1021/ic4029589

Nanocomposite $YCrO_3/Al_2O_3$: Characterization of the Core–Shell, Magnetic Properties, and Enhancement of Dielectric Properties

A. Durán,* H. Tiznado, J. M. Romo-Herrera, D. Domínguez, R. Escudero, and J. M. Siqueiros

Alumina-coated multiferroic particles are promising architecture to improve the functional bulk ceramics. The Y@Al nanocomposite was fabricated by atomic-layer deposition. The Al_2O_3 shell on the $YCrO_3$ particles serves as a barrier layer. This is because the Al_2O_3 shell localizes the charge carriers, reducing the loss tangent and decreasing the electrical conductivity. The Y@Al array proves that the free charges at the grain boundaries are mainly responsible for the degradation of the hysteresis loops in bulk multiferroics.

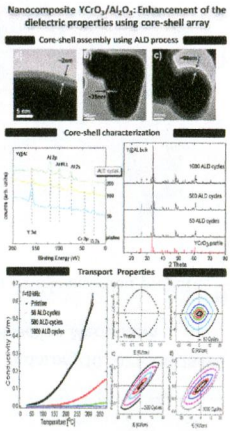

4881 S dx.doi.org/10.1021/ic402953s

Acetylcholine-like and Trimethylglycine-like PTA (1,3,5-Triaza-7-phosphaadamantane) Derivatives for the Development of Innovative Ru- and Pt-Based Therapeutic Agents

Valeria Ferretti, Marco Fogagnolo, Andrea Marchi, Lorenza Marvelli, Fabio Sforza, and Paola Bergamini*

Novel PTA *N*-alkyl derivatives presenting all the functional groups of the natural cationic compounds acetylcholine or trimethylglycine, combined with a P-donor site suitable for metal ion coordination, have been prepared and coordinated to platinum and ruthenium for use as anticancer agents. The X-ray crystal structure of $[CpRu(PPh_3)(PTAC_2H_4OCOMe)Cl]PF_6$ (**1cRu**) was determined. The antiproliferative activity of ligands and complexes was evaluated on three human cancer cell lines.

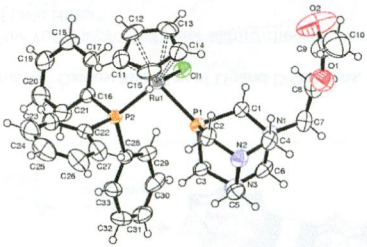

4891 S dx.doi.org/10.1021/ic402994q

Synthesis and Characterization of Novel Wells–Dawson-Type Mono Vanadium(V)-Substituted Tungsto-polyoxometalate Isomers: 1- and 4-$[S_2VW_{17}O_{62}]^{5-}$

Tadaharu Ueda,* Miho Ohnishi, Motoo Shiro, Jun-ichi Nambu, Toshiaki Yonemura, John F. Boas, and Alan M. Bond

Two Wells–Dawson-type vanadium(V)-substituted tungsto-polyoxometalate isomers, 1- and 4-$[S_2VW_{17}O_{62}]^{5-}$, were prepared as their tetra-alkyl ammonium salts from a W^{VI}–H_2SO_4–V^V reaction mixture in aqueous CH_3CN solution. The isomers were characterized by elemental analysis, X-ray crystallography, and infrared, Raman, UV–vis, ^{51}V, and NMR spectroscopies as well as voltammetry, and the data obtained were compared with that derived from $[S_2W_{18}O_{62}]^{4-}$. The one-electron-reduced $[S_2V^{IV}W_{17}O_{62}]^{6-}$ form of both isomers were characterized by voltammetry and EPR spectroscopy.

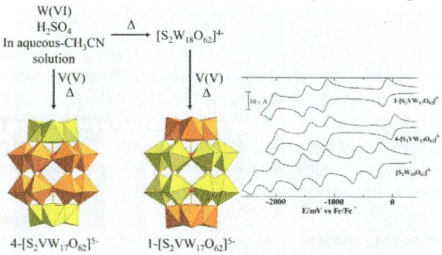

4899 S dx.doi.org/10.1021/ic403043e

Reactivity of Biomimetic Iron(II)-2-aminophenolate Complexes toward Dioxygen: Mechanistic Investigations on the Oxidative C–C Bond Cleavage of Substituted 2-Aminophenols

Biswarup Chakraborty, Sourav Bhunya, Ankan Paul, and Tapan Kanti Paine*

Iron(II)-2-aminophenolate complexes of a N_4 ligand react with O_2 to cleave the C–C bond of 2-aminophenolates regioselectively. The nature of substitution on the aminophenolate ring directs the reactivity of the iron(II) complexes.

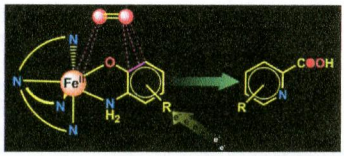

4913 S dx.doi.org/10.1021/ic403067h

Influence of Aqueous Precursor Chemistry on the Growth Process of Epitaxial $SrTiO_3$ Buffer Layers

Glenn Pollefeyt, Sander Clerick, Pieter Vermeir, Petra Lommens, Klaartje De Buysser, and Isabel Van Driessche*

Epitaxial thin films of $SrTiO_3$ were prepared on (100) $LaAlO_3$ substrates by an aqueous chemical solution deposition method. It was observed that the interaction of the metal ions with the chelating agents used to stabilize the metal ions in water had a strong influence on the morphological properties of the obtained $SrTiO_3$ fully heat treated thin films. Precursor solutions in which both metal ions were stabilized gave rise to preferentially textured, dense, and terraced $SrTiO_3$ films, allowing subsequent deposition of $YBa_2Cu_3O_{7-\delta}$ with superior superconducting performances.

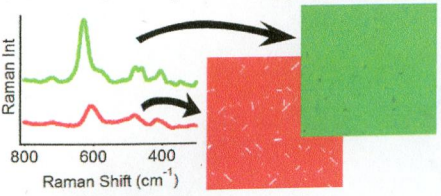

4922 S dx.doi.org/10.1021/ic403113z

Synthesis and Characterization of ^{68}Ga-Labeled Curcumin and Curcuminoid Complexes as Potential Radiotracers for Imaging of Cancer and Alzheimer's Disease

Mattia Asti,* Erika Ferrari, Stefania Croci, Giulia Atti, Sara Rubagotti, Michele Iori, Pier C. Capponi, Alessandro Zerbini, Monica Saladini, and Annibale Versari

A series of metal complexes of stoichiometry $M(L)_2^+$ in which curcumin and two curcumin derivatives (diacetyl-curcumin and bis(dehydroxy)curcumin) act as OO bidentate ligand for the positron-emitting radionuclide gallium-68 were synthesized and characterized. Because of their biological properties in vitro, the ^{68}Ga-curcuminoid complexes show potential as diagnostic radiotracers for cancer and Alzheimer's disease.

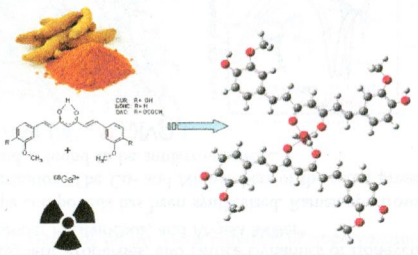

4934 S dx.doi.org/10.1021/ic4031238

Photochemical Redox Reactions of Copper(II)–Alanine Complexes in Aqueous Solutions

Chen-Jui Lin, Chao-Sheng Hsu, Po-Yen Wang, Yi-Liang Lin, Yu-Shiu Lo, and Chien-Hou Wu*

Quantum yields of Cu(I), ammonia, and acetaldehyde for individual Cu(II)/alanine complexes at 313 nm were determined and characterized mainly with the equilibrium Cu(II) speciation where the presence of CuL and CuL_2 is taken into account. In view of the Cu(II)-complex stoichiometry, CuL always has larger quantum yields than CuL_2, which implies that the photoreactivities of Cu(II)/amino acid complexes could be underestimated in natural aquatic systems.

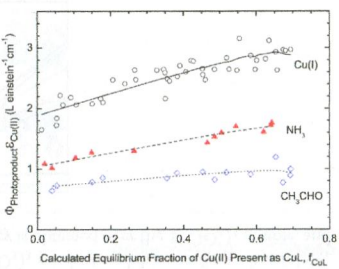

4944 Ⓢ dx.doi.org/10.1021/ic403149b

A Schiff Base and Its Copper(II) Complex as a Highly Selective Chemodosimeter for Mercury(II) Involving Preferential Hydrolysis of Aldimine over an Ester Group

Ashish Kumar, Mrigendra Dubey, Rampal Pandey, Rakesh Kumar Gupta, Amit Kumar, Alok Ch. Kalita, and Daya Shankar Pandey*

Synthesis, characterization, X-ray single-crystal structures, and chemodosimeter behavior of a new Schiff base, diethyl-5-(2-hydroxybenzylidene)aminoisophthalate (**HL**), and its copper complex, $[\mathbf{Cu(L_2)}]$ (**1**), have been described. The discrete chemodosimetric nature of **HL** and **1** toward Hg^{2+} has been established by UV/vis, emission, and mass spectral studies. Comparative studies between **HL** and **1** further demonstrated that the chemodosimetric response merely initiates from specific hydrolysis of the aldimine core over ester groups. The ultimate product after hydrolysis has been identified as diethyl-5-aminoisophthalate, being one of the reactants in **HL**. The sensitivity of these chemodosimeters toward Hg^{2+} has been estimated within an acceptable level (8×10^{-10} M) with excellent selectivity.

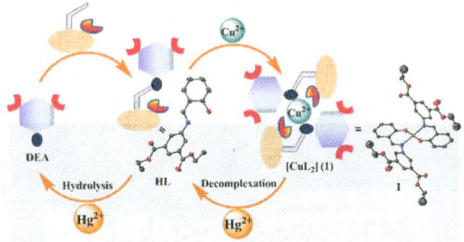

4956 Ⓢ dx.doi.org/10.1021/ic403134c

Isomeric Ionic Lithium Isonicotinate Three-Dimensional Networks and Single-Crystal-to-Single-Crystal Rearrangements Generating Microporous Materials

Brendan F. Abrahams,* A. David Dharma, Martin J. Grannas, Timothy A. Hudson, Helen E. Maynard-Casely, Graham R. Oliver, Richard Robson,* and Keith F. White

The crystallization of a lithium salt of a simple organic anion, in the presence of templating solvents, leads to the formation of 3D ionic networks that are able to undergo desolvation to yield a porous network with different connectivity. These transformations, some reversible, are able to occur with retention of single-crystal character. The ability of these compounds to undergo major structural rearrangements is attributed to the "plasticity" of the interactions in the ionic networks.

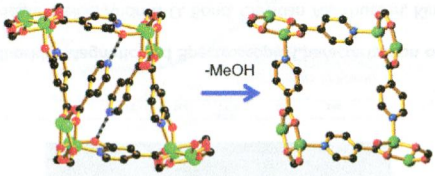

4970 Ⓢ dx.doi.org/10.1021/ic403167m

Redox-Active Porous Coordination Polymers Prepared by Trinuclear Heterometallic Pivalate Linking with the Redox-Active Nickel(II) Complex: Synthesis, Structure, Magnetic and Redox Properties, and Electrocatalytic Activity in Organic Compound Dehalogenation in Heterogeneous Medium

A. S. Lytvynenko, S. V. Kolotilov,* M. A. Kiskin, O. Cador, S. Golhen, G. G. Aleksandrov, A. M. Mishura, V. E. Titov, L. Ouahab, I. L. Eremenko,* and V. M. Novotortsev

New redox-active porous coordination polymer was prepared by linking of the trinuclear pivalate $Fe_2CoO(Piv)_6$ by the redox-active bridge complex $Ni^{II}(L)_2$ with Schiff base. Formation of such polymer led to minor changes of electronic structure of $Ni(L)_2$, as can be concluded from analysis of magnetic data and the values of redox potentials. Electrocatalytic activity of the coordination polymer in dehalogenation of organic compounds was studied.

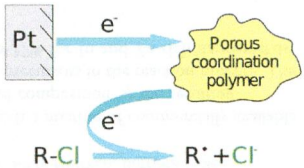

4980 S dx.doi.org/10.1021/ic403122j

Studies of Cobalt-Mediated Electrocatalytic CO_2 Reduction Using a Redox-Active Ligand

David C. Lacy, Charles C. L. McCrory, and Jonas C. Peters*

Electrocatalytic CO_2 reduction was achieved using a homogeneous molecular cobalt complex in MeCN with 10 M H_2O using a glassy carbon working electrode. Control experiments and XPS measurements of the working electrode strongly suggest that the catalysis involves a molecular species rather than heterogeneous material. In addition to catalysis, stoichiometric reduction of the precatalyst resulted in the formation of several new reduced compounds in which the electronic structures were probed with XRD and DFT.

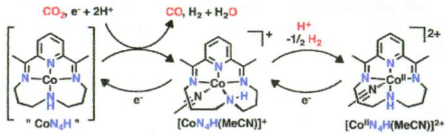

4989 S dx.doi.org/10.1021/ic500027f

$Ln(IO_3)_3$ (Ln = Ce, Nd, Eu, Gd, Er, Yb) Polycrystals As Novel Photocatalysts for Efficient Decontamination under Ultraviolet Light Irradiation

Wenjun Wang, Hefeng Cheng, Baibiao Huang,* Xinru Li, Xiaoyan Qin, Xiaoyang Zhang, and Ying Dai

A simple hydrothermal method was used to sythesize $Ln(IO_3)_3$ (Ln = Ce, Nd, Eu, Gd, Er, Yb) polycrystals. All the $Ln(IO_3)_3$ products have strong absorption in the ultraviolet region. The as-prepared $Ln(IO_3)_3$ products exhibit excellent ultraviolet-light-driven photocatalytic activities toward degradation of MO. The highest activity is obtained over the $Yb(IO_3)_3$ sample, and about 77% of MO is decomposed after irradiation for 1 h.

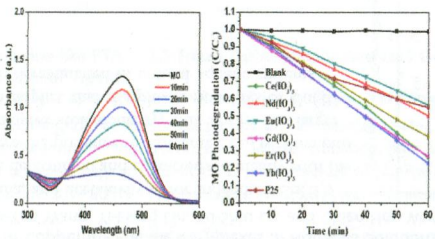

4994 S dx.doi.org/10.1021/ic500028b

$AAg_2(M'_{1/3}M_{2/3})[VO_4]_2$: Synthesis, Magnetic Properties, and Lattice Dynamics of Honeycomb-Type Lattices

Michaela Bratsch, Joshua Tapp, Alexander P. Litvinchuk, and Angela Möller*

A series of magnetic honeycomb type compounds has been synthesized. Raman spectroscopy and magnetic measurements have been employed in the characterization. The Co- and Ni-members of the series present examples for ferromagnetic insulators, whereas the Mn-compound is found to be antiferromagnetic.

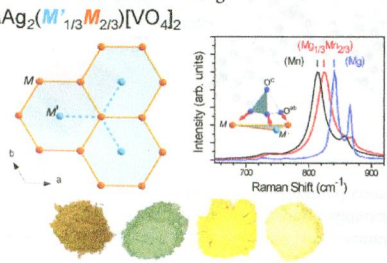

5002 S dx.doi.org/10.1021/ic500046m

A Simple Route to Alloyed Quaternary Nanocrystals Ag–In–Zn–S with Shape and Size Control

Grzegorz Gabka, Piotr Bujak,* Kamila Giedyk, Andrzej Ostrowski, Karolina Malinowska, Jerzy Herbich, Barbara Golec, Ireneusz Wielgus, and Adam Pron

The preparation of alloyed quaternary Ag–In–Zn–S nanocrystals is elaborated, in which a mixture of commercially available precursors is used with 1-octadecene as a solvent. In these conditions shape, size, and composition of the resulting nanocrystals can be adjusted in a controlled manner by changing the molar ratio of the precursors in the reaction mixture. The prepared nanoparticles show stable photoluminescence with the quantum yield up to 37% for In and Zn-rich nanocrystals.

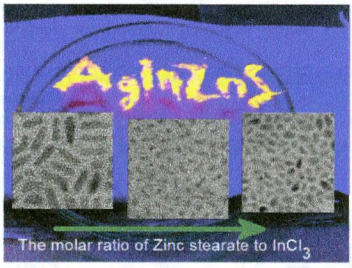

5013 S dx.doi.org/10.1021/ic500049w

Magnetic Interactions through Fluoride: Magnetic and Spectroscopic Characterization of Discrete, Linearly Bridged $[Mn^{III}_2(\mu\text{-}F)F_4(Me_3tacn)_2](PF_6)$

Kasper S. Pedersen, Marc Sigrist, Høgni Weihe, Andrew D. Bond, Christian Aa. Thuesen, Kim P. Simonsen, Torben Birk, Hannu Mutka, Anne-Laure Barra, and Jesper Bendix*

The magnetic interaction through a linear fluoride bridge along the Jahn–Teller axis of a dinuclear manganese(III) complex is scrutinized. High-frequency electron paramagnetic resonance, neutron scattering, magnetometry and electronic spectroscopy are supplemented by density functional theory computations. The exchange coupling strength is smaller than that found in comparable systems with linear oxide bridging but comparable to magnitudes for cyanide-bridged systems.

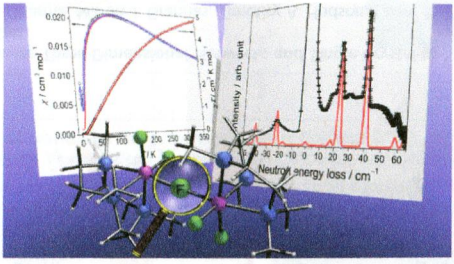

5020 dx.doi.org/10.1021/ic500052v

Molecular Magnets Based on Homometallic Hexanuclear Lanthanide(III) Complexes

Sourav Das, Sakiat Hossain, Atanu Dey, Sourav Biswas, Jean-Pascal Sutter,* and Vadapalli Chandrasekhar*

The synthesis, structure, and magnetic properties of hexanuclear lanthanide complexes having a $[Ln_6(OH)_4]^{14+}$ core consisting of four fused $[Ln_3(OH)]^{8+}$ subunits are reported. Both static (dc) and dynamic (ac) magnetic properties of all complexes have been studied. Single-molecule magnetic behavior has been observed in the Dy_6 analogue with an effective energy barrier and relaxation time of $\Delta/k_B = 46.2$ K and $\tau_0 = 2.85 \times 10^{-7}$ s, respectively.

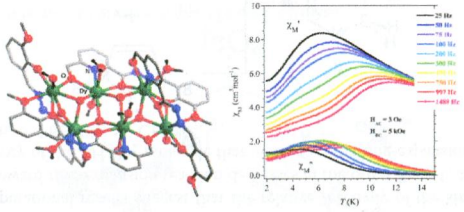

5029 dx.doi.org/10.1021/ic500062j

Symmetry Breaking of α-$[H_2W_{12}O_{40}]^{6-}$ Depends on the Transformation of Isopolyoxotungstates

Ying-Nan Chi, Pan-Pan Shen, Feng-Yun Cui, Zheng-Guo Lin, Shi-Lu Chen,* and Chang-Wen Hu*

The enantiomers $[Cu_3(L1)_3(H_2O)_2(H_2W_{12}O_{40})]\cdot 4H_2O$ (**1a,b**) were spontaneously isolated without any chiral auxiliary. Control experiments show that their formation depends on the transformation of isopolyoxotungstates. The possible reaction intermediate $Cu_3(L1)_3(H_2O)_3[H_4W_{11}O_{38}]$ as a precursor for **1a,b** has been presented and characterized by density functional theory (DFT) calculations.

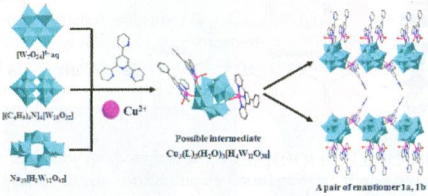

5037 dx.doi.org/10.1021/ic500066p

Peroxido Complexes of Vanadium(V) as Ligands. Crystal Structures of $[Cd(NH_3)_6][\{VO(O_2)_2(OH)\}_2\{\mu\text{-}Cd(NH_3)_4\}]$ and $[\{VO(O_2)_2(Im)\}_2\{\mu\text{-}Cu(Im)_4\}]$ (Im = Imidazole)

Roman Bystrický, Peter Antal, Jozef Tatiersky,* Peter Schwendt, Róbert Gyepes, and Zdirad Žák

Compounds containing trinuclear heterometallic complexes with coordinated diperoxidovanadium moieites were synthesized and characterized by spectral methods and X-ray crystallography.

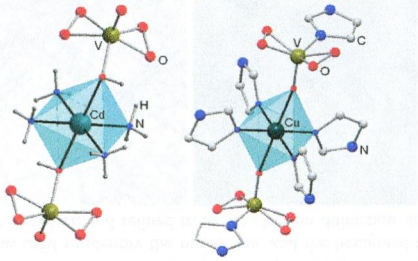

5044 Ⓢ dx.doi.org/10.1021/ic500092t

Regulation of Aggregation Behavior and Neurotoxicity of Prion Neuropeptides by Platinum Complexes

Xuesong Wang, Menghan Cui, Cong Zhao, Lei He, Dengsen Zhu, Baohuai Wang, and Weihong Du*

Platinum complexes in the form of L-$PtCl_2$ effectively inhibit the aggregation of PrP106−126 and its mutants. The ligand configuration contributes to both the binding affinity and the inhibition of peptide aggregation.

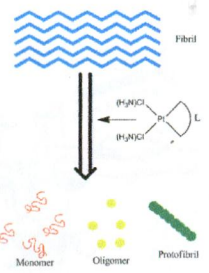

5055 Ⓢ dx.doi.org/10.1021/ic5001057

Solvate-Dependent Spin Crossover and Exchange in Cobalt(II) Oxazolidine Nitroxide Chelates

Ian A. Gass, Subrata Tewary, Gopalan Rajaraman, Mousa Asadi, David W. Lupton, Boujemaa Moubaraki, Guillaume Chastanet, Jean-Francois Létard, and Keith S. Murray*

The complexes $[Co^{II}(L^{\bullet})_2](B(C_6F_5)_4)_2{\cdot}CH_2Cl_2$ (**1**) and $[Co^{II}(L^{\bullet})_2](B(C_6F_5)_4)_2{\cdot}2Et_2O$ (**2**) ($L^{\bullet}$ = 4,4-dimethyl-2,2-bis(pyridin-2-yl)oxazolidine *N*-oxide) have been investigated using variable-temperature X-ray structure analysis, magnetic susceptibility and optical reflectivity measurements, and density functional theory (DFT) calculations. Complex **1** shows simultaneous exchange and spin crossover with theoretical studies revealing that the exchange is sensitive to the tilt angle (θ) between the Co(d_{z^2}) orbital and the O atom from the nitroxide NO moiety in $L^{\bullet}$. Complex **2** remains high spin throughout, with exchange coupling.

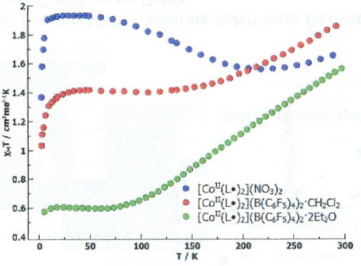

5067 dx.doi.org/10.1021/ic500056r

Phase Identification and Structure Solution by Three-Dimensional Electron Diffraction Tomography: Gd–Phosphate Nanorods

Arnaud Mayence, Julien R. G. Navarro, Yanhang Ma, Osamu Terasaki, Lennart Bergström, and Peter Oleynikov*

Hydrothermal synthesis was employed to obtain $GdPO_4$ nanorods with an aspect ratio of 20. Three-dimensional electron diffraction tomography (3D EDT) was used to identify the monoclinic and the hexagonal forms from individual $GdPO_4$ nanorods. Both crystal structures were resolved and refined from 3D electron diffraction data sets.

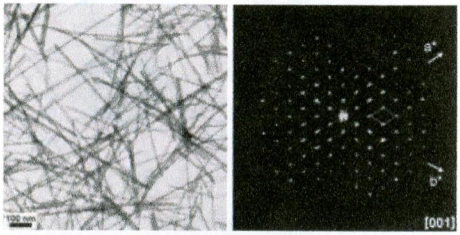

5073 dx.doi.org/10.1021/ic500116f

Are Ligand-Stabilized Carboxylic Acid Derivatives with Ge=Te Bonds Isolable?

Rahul Kumar Siwatch, Dhirendra Yadav, Goutam Mukherjee, Gopalan Rajaraman, and Selvarajan Nagendran*

Ligand-stabilized carboxylic acid derivatives such as germatelluroester [LGe(Te)O*t*-Bu] (**4**), germatelluroamide [LGe(Te)-$N(SiMe_3)_2$] (**5**), and germatelluroacid anhydride [LGe(Te)OGe(Te)L] (**6**) are isolated for the first time through the oxidative addition of elemental tellurium to the corresponding germylenes **1**, **2**, and **3**, respectively. Compounds **4**–**6** are structurally characterized, and the nature of the bonding in the (Te)GeO*t*-Bu, (Te)GeN$(SiMe_3)_2$, and (Te)GeOGe(Te) moieties is probed by theoretical studies.

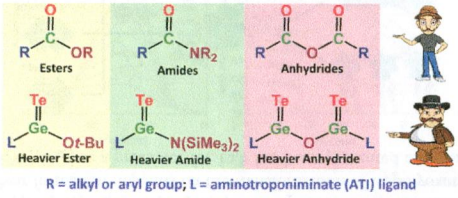

5080 dx.doi.org/10.1021/ic500182f

Mechanistic Investigations on E–N Bond-Breaking and Ring Expansion for *N*-Heterocyclic Carbene Analogues Containing the Group 14 Elements (E)

Ming-Der Su*

The M06-2X/Def2-TZVP computational results suggest that the relative reactivity of the six-valence-electron *N*-heterocyclic tetrelylidene species (**Rea–E**) toward ring-expansion reaction decreases in the order **Rea–C** ≫ **Rea–Si** > **Rea–Ge** > **Rea–Sn** > **Rea–Pb**. However, the reactivity of the EH_2Ph_2 molecule that undergoes the ring-expansion reaction decreases in the order $SiH_2Ph_2 \approx GeH_2Ph_2 \approx SnH_2Ph_2 > PbH_2Ph_2 \gg CH_2Ph_2$.

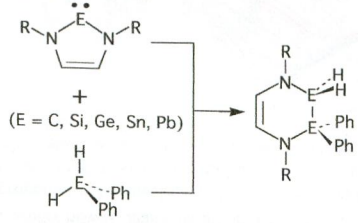

5088 dx.doi.org/10.1021/ic500200a

Lattice Parameters and Stability of the Spinel Compounds in Relation to the Ionic Radii and Electronegativities of Constituting Chemical Elements

Mikhail G. Brik,* Andrzej Suchocki, and Agata Kamińska

Lattice parameters of 185 binary and ternary spinel compounds were modeled as a function of the ionic radii and electronegativities of the constituting ions. A simple empirical equation was found, which yields good agreement between the experimental and modeled values of the lattice parameters, with an average error of about 1% only. The obtained results offer a systematic overview of spinels structural properties and can serve as helpful guides for synthesis of new spinel compounds.

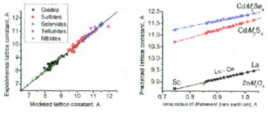

5100 S dx.doi.org/10.1021/ic500195q

Aluminum-Stabilized Low-Spin Iron(II) Hydrido Complexes of 1,4,7-Trimethyl-1,4,7-triazacyclononane

Masataka Oishi, Togo Endo, Masato Oshima, and Hiroharu Suzuki*

Low-spin 1,4,7-trimethyl-1,4,7-triazacyclononane (Me_3tacn) iron(II) hydrides (**2**–**4**) stabilized by aluminum were synthesized from $(Me_3tacn)FeCl_n$ (**1**; n = 2, 3) and several aluminum hydride reagents. The short Fe–Al distances were probed using DFT calculations, which indicated the electron-donating nature of the Me_3tacn-iron(II) hydrido fragment toward the aluminum(III) center.

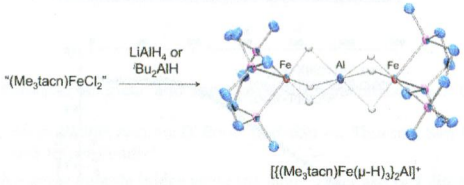

5109 S dx.doi.org/10.1021/ic5002122

Structurally Diverse Copper Complexes Bearing NNO-Tridentate Schiff-Base Derivatives as Efficient Catalysts for Copolymerization of Carbon Dioxide and Cyclohexene Oxide

Chen-Yen Tsai, Bor-Hunn Huang, Mon-Wei Hsiao, Chu-Chieh Lin,* and Bao-Tsan Ko*

We report the first use of bimetallic copper acetate complex **3** bearing NNO-tridentate Schiff-base ligands as an efficient catalyst for CHO/CO_2 copolymerization in a controlled character, producing polymers with controllable molecular weights and a highly alternating microstructure up to 96% carbonate linkages.

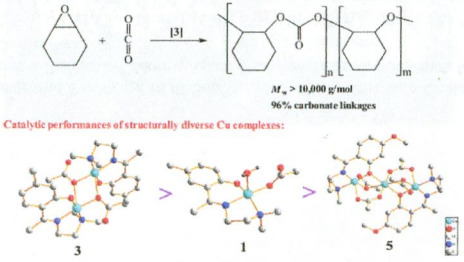

5117 Ⓢ dx.doi.org/10.1021/ic500229r

Fluoridonitrosyl Complexes of Technetium(I) and Technetium(II). Synthesis, Characterization, Reactions, and DFT Calculations

Samundeeswari Mariappan Balasekaran, Johann Spandl, Adelheid Hagenbach, Klaus Köhler, Markus Drees, and Ulrich Abram*

A number of low-valent nitrosyltechnetium complexes with fluorido ligands was synthesized from $M_2[Tc(NO)F_5]$ (M = K, Rb) and $[Tc(NO)(NH_3)_4F](X)$ (X = HF_2, PF_6) complexes, which can readily be accessed from pertechnetate by reactions with acetohydroxamic acid in HF. The products were isolated in crystalline form and studied by X-ray diffraction and spectroscopically. The Tc−F bonds are remarkably stable against hydrolysis.

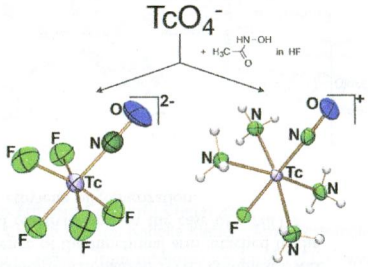

5129 Ⓢ dx.doi.org/10.1021/ic500230v

New Yellow-Emitting Whitlockite-type Structure $Sr_{1.75}Ca_{1.25}(PO_4)_2:Eu^{2+}$ Phosphor for Near-UV Pumped White Light-Emitting Devices

Haipeng Ji, Zhaohui Huang,* Zhiguo Xia,* Maxim S. Molokeev, Victor V. Atuchin, Minghao Fang, and Saifang Huang

A new yellow-emitting whitlockite-type structure phosphor $Sr_{1.75}Ca_{1.25}(PO_4)_2:Eu^{2+}$ was reported. Crystal structure is refined to be rhombohedral unit cell with space group *R*3c and lattice constants a = 10.6498(3) Å and c = 38.787(1) Å, and cell volume = 3809.8(2) Å^3. It exhibits a broad emission band peaking at 514 nm, showing a large red-shift compared with the Eu^{2+} doped $Sr_3(PO_4)_2$ and $Ca_3(PO_4)_2$ blue phosphors.

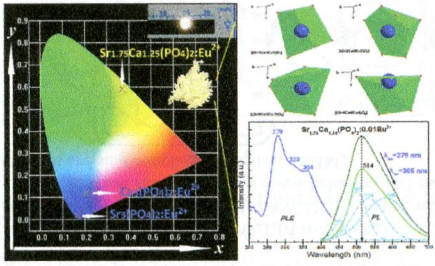

5136 dx.doi.org/10.1021/ic500231z

Picolinate-Containing Macrocyclic Mn^{2+} Complexes as Potential MRI Contrast Agents

Enikő Molnár, Nathalie Camus, Véronique Patinec, Gabriele A. Rolla, Mauro Botta, Gyula Tircsó,* Ferenc K. Kálmán, Tamás Fodor, Raphaël Tripier,* and Carlos Platas-Iglesias*

A series of Mn^{2+} complexes based on triaza- or tetraaza-macrocyclic platforms that contain a picolinate pendant arm have been investigated. Potentiometric and spectroscopic measurements have been conducted to assess the thermodynamic and kinetic stability of these complexes. ^{1}H NMRD and ^{17}O NMR measurements show that the complex with a tacn-based ligand contains one water molecule coordinated to the Mn^{2+} ion endowed with a very fast exchange rate (see Abstract Graphic).

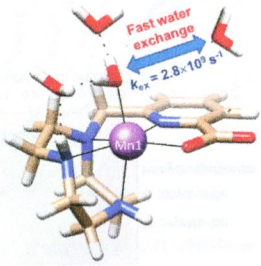

5150 dx.doi.org/10.1021/ic500250e

Subcellular Localization and Transport Kinetics of Ruthenium Organometallic Anticancer Compounds in Living Cells: A Dose-Dependent Role for Amino Acid and Iron Transporters

M. Klajner, C. Licona, L. Fetzer, P. Hebraud, G. Mellitzer, M. Pfeffer, S. Harlepp,* and C. Gaiddon*

Luminescent properties of organoruthenium (Ru(II)) compounds obtained with a cyclometalated 2-phenylpyridine chelate and aromatic chelating ligands showed a difference in sensitivity toward cancerous and noncancerous cells, with one compound following a balance between active and passive transport. The active-transport mechanism seems to be transcriptionally regulated. Additionally, a correlation was established between the accumulation of these compounds in endoplasmic reticulum, nucleus, and mitochondria and the activation of cytotoxic mechanisms such as the mitochondrial stress pathway.

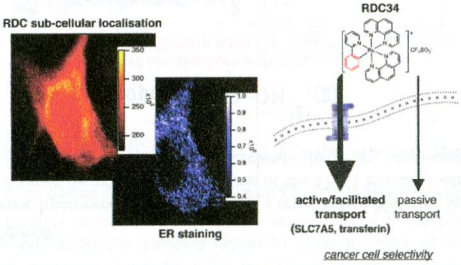

5159 dx.doi.org/10.1021/ic500259k

Digallane with Redox-Active Diimine Ligand: Dualism of Electron-Transfer Reactions

Igor L. Fedushkin,* Alexandra A. Skatova, Vladimir A. Dodonov, Valentina A. Chudakova, Natalia L. Bazyakina, Alexander V. Piskunov, Serhiy V. Demeshko, and Georgy K. Fukin

A dual reactivity of diimine gallium complex (dpp-Bian)Ga–Ga(dpp-Bian) consistsing of redox-active ligand 1,2-bis[(2,6-diisopropylphenyl)imino]acenaphthene (dpp-Bian) toward various oxidants has been disclosed. It has been demonstrated that in the reactions with iodine and benzylideneacetone an oxidation of the dianionic dpp-Bian ligands to radical-anionic state takes place before oxidation of the metal–metal bond. The reaction of digallane with 3,6-di-*tert*-butyl-*ortho*-benzoquinone proceeds with oxidation of the Ga–Ga bond as well as of two dpp-Bian dianions.

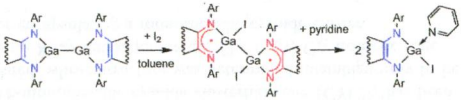

5171 dx.doi.org/10.1021/ic500267b

Tridentate Benzimidazole-Pyridine-Tetrazolates as Sensitizers of Europium Luminescence

Nail M. Shavaleev,* Svetlana V. Eliseeva, Rosario Scopelliti, and Jean-Claude G. Bünzli*

"Soft" tridentate benzimidazole-pyridine-tetrazolates efficiently sensitize the europium luminescence despite weaker bonding compared to "hard" carboxylate analogues.

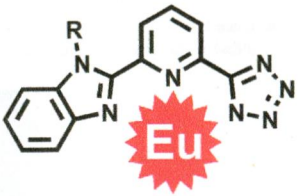

5179 dx.doi.org/10.1021/ic500298u

Multinuclear Cobalt(II)-Containing Heteropolytungstates: Structure, Magnetism, and Electrochemistry

Masooma Ibrahim, Ali Haider, Yanhua Lan, Bassem S. Bassil, Akina M. Carey, Rongji Liu, Guangjin Zhang, Bineta Keita, Wenhui Li, George E. Kostakis, Annie K. Powell, and Ulrich Kortz*

The 16-cobalt(II)-containing heteropolytungstates $[\{Co_4(OH)_3PO_4\}_4(A\text{-}\alpha\text{-}XW_9O_{34})_4]^{32-}$ (X = Si, Ge) comprise a cationic $\{Co_{16}(OH)_{12}(PO_4)_4\}^{8+}$ assembly stabilized by four trilacunary $\{A\text{-}\alpha\text{-}XW_9O_{34}\}^{10-}$ units, resulting in an overall tetrahedral structure. The electrochemistry studies in solution showed exciting redox behavior, and the magnetic properties in the solid state demonstrated that both compounds are single-molecule magnets (SMM).

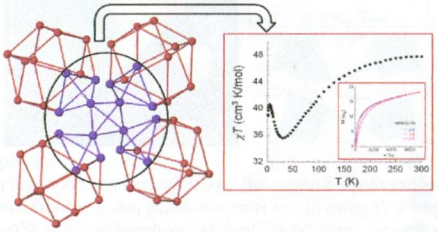

5189 dx.doi.org/10.1021/ic500349t

Synthesis and Characterization of Palladium(II) and Nickel(II) Alcoholate-Functionalized NHC Complexes and of Mixed Nickel(II)−Lithium(I) Complexes

Sophie Hameury, Pierre de Frémont, Pierre-Alain R. Breuil, Hélène Olivier-Bourbigou, and Pierre Braunstein*

The synthesis of Pd(II) and Ni(II) alcohol-functionalized NHC complexes was explored to examine the possible influence of the functional arm attached to the NHC backbone on their structure and reactivity and, in the case of a Ni(II) complex, on its catalytic properties in ethylene oligomerization.

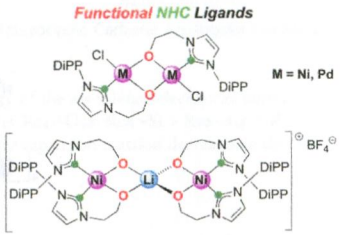

5201 dx.doi.org/10.1021/ic500353k

Putting a Terbium-Monometallic Cyanide Cluster into the C_{82} Fullerene Cage: TbCN@C_2(5)-C_{82}

Fupin Liu, Song Wang, Jian Guan, Tao Wei, Minxiang Zeng, and Shangfeng Yang*

TbCN@C_2(5)-C_{82} as the first Tb-monometallic cyanide clusterfullerene (CYCF) has been successfully synthesized and isolated, whose structure was determined unambiguously to be TbCN@C_2(5)-C_{82} by single crystal X-ray diffraction study. The C_2(5)-C_{82} isomeric cage represents a new cage capable of encapsulating a monometallic cyanide cluster.

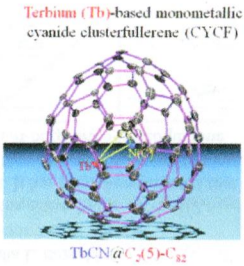

5206 dx.doi.org/10.1021/ic5003786

Kinetic Analysis of the Formation and Decay of a Non-Heme Ferric Hydroperoxide Species Susceptible to O–O Bond Homolysis

Qiao Zhang and Christian R. Goldsmith*

The formation and decay of a ferric hydroperoxide complex with a tetradentate N-donor ligand was studied using stopped-flow techniques. Fe^{III}–OOH undergoes decay through homolysis of the O–O bond. Substrates that had previously been shown to be oxidized under the reaction conditions failed to accelerate the decay, suggesting that Fe^{III}–OOH is not directly responsible for the oxidation of their C–H bonds.

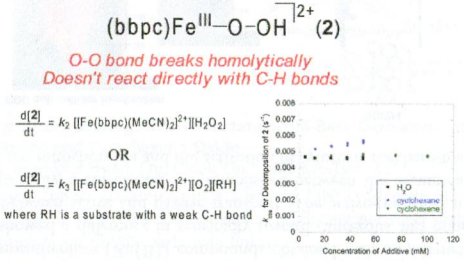

5212 dx.doi.org/10.1021/ic500403v

Oxychloride–Hydroxychloride–Trihydroxide Phase Relationships of Rare Earths in Aqueous Solution

Byung-Il Lee, Heejin Jeong, and Song-Ho Byeon*

In-depth exploration of the hydrolysis behavior of REOCls provided systematic phase diagrams for rare earth oxychloride–water systems that can be used as guidelines for the preparation and application of REOCls and $RE_2(OH)_5Cl{\cdot}nH_2O$ phases in aqueous media.

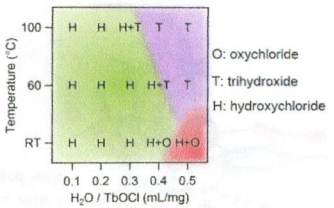

5222 S dx.doi.org/10.1021/ic5004116

Series of Lead Oxide Hydroxide Nitrates Obtained by Adjusting the pH Values of the Reaction Systems

Genxiang Wang, Min Luo, Ning Ye,* Chensheng Lin, and Wendan Cheng

A series of lead oxide hydroxide nitrates has been obtained by adjusting the pH values of the $Pb(NO_3)_2$–NaOH system. The pH value of the reaction system makes a difference in the structure of the resultants. With the rise of pH value, the ratio of Pb/OH in the molecular formula of these compounds increases, which results in the diversity of structures.

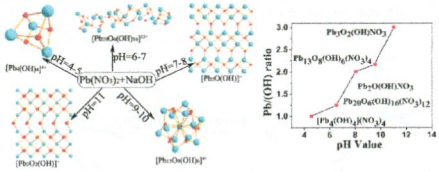

5229 S dx.doi.org/10.1021/ic5004319

D-Penicillamine Tripodal Derivatives as Efficient Copper(I) Chelators

Anne-Solène Jullien, Christelle Gateau, Colette Lebrun, Isabelle Kieffer, Denis Testemale, and Pascale Delangle*

Promising tripodal chelating architectures derived from nitrilotriacetic acid (NTA) were built from three unnatural amino acids D-penicillamine (D-Pen). The hindrance of this bulkier analogue of cysteine is demonstrated to influence the speciation and stability of the Cu(I) complexes. The two D-Pen derivatives bind Cu(I) tightly and selectively in trigonal-planar sulfur-only environments in either mononuclear complexes CuL or in $(Cu_2L)_2$ clusters, with Cu_4S_6 cores evidenced in complexes with metallothioneins.

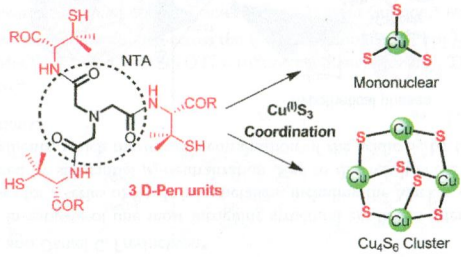

5240 S dx.doi.org/10.1021/ic5004337

Strong Second Harmonic Generation (SHG) Originating from Combined Second-Order Jahn–Teller (SOJT) Distortive Cations in a New Noncentrosymmetric Tellurite, $InNb(TeO_4)_2$

Yeong Hun Kim, Dong Woo Lee, and Kang Min Ok*

The strong second harmonic generation efficiency of $InNb(TeO_4)_2$ is attributable to the combined net polarization arising from the distorted coordination environment of second-order Jahn–Teller (SOJT) distortive cations: i.e., Nb^{5+} and Te^{4+}.

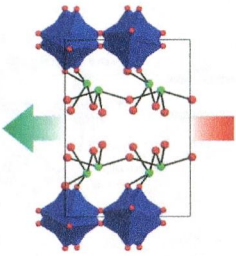

5246 S dx.doi.org/10.1021/ic500463m

Co-ligand and Solvent Effects on the Spin-Crossover Behaviors of PtS-type Porous Coordination Polymers

Xiang-Yi Chen, Rong-Bin Huang, Lan-Sun Zheng, and Jun Tao*

Three two-fold interpenetrated PtS-type porous coordination polymers, $[Fe(X)_2(tppm)]\cdot S$ [tppm = 4,4′,4″,4‴-tetrakis(4-pyridylethen-2-yl)tetraphenylmethane, $S = 5CH_3OH{\cdot}2CH_2Cl_2$; X = $NCSe^-$, **2**·*S*; $NCBH_3^-$, **3**·*S*; $N(CN)_2^-$, **4**·*S*], showing spin-crossover behaviors that can be tuned by co-ligands and solvent molecules are reported.

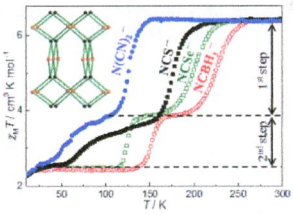

5253 S dx.doi.org/10.1021/ic500466w

Synthesis, Crystal Structure, and High-Temperature Phase Transition of the Novel Plumbide Na_2MgPb

Takahiro Yamada,* Takuji Ikeda, Ralf P. Stoffel, Volker L. Deringer, Richard Dronskowski, and Hisanori Yamane

Na_2MgPb was synthesized, and the compound exhibits three polymorphs (α, β, γ). The $\alpha \rightarrow \beta$ and $\beta \rightarrow \gamma$ phase transitions occur at 493–543 and 533–633 K. The molar volume of the γ phase is 9–13% smaller than those of the α and β phases. DFT calculations suggest that an inverse Heusler-type structure is plausible for the γ phase, and correctly reproduce the $\alpha \rightarrow \gamma$ phase transition albeit at higher temperature than seen experimentally.

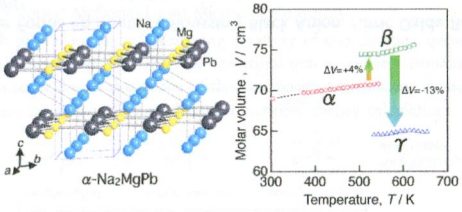

5260 S dx.doi.org/10.1021/ic500479e

Perovskite Metal Formate Framework of $[NH_2\text{-}CH^+\text{-}NH_2]Mn(HCOO)_3$: Phase Transition, Magnetic, Dielectric, and Phonon Properties

Mirosław Mączka,* Aneta Ciupa, Anna Gągor, Adam Sieradzki, Adam Pikul, Bogusław Macalik, and Marek Drozd

We report the synthesis and temperature-dependent studies of a perovskite metal formate framework of $[NH_2\text{-}CH^+\text{-}NH_2][Mn(HCOO)_3]$. This compound undergoes a slightly first-order phase transition at around 335 K associated with ordering of the FMD^+ cations and symmetry change from $R\bar{3}c$ to $C2/c$. In contrast to closely related multiferroic $[(CH_3)_2NH_2][Mn(HCOO)_3]$, the phase transition is associated with very weak distortion and tilting of the organic cation.

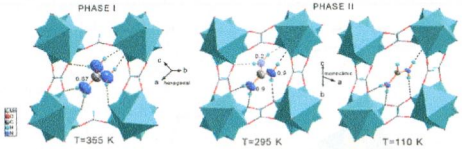

5269 Ⓢ dx.doi.org/10.1021/ic500491c

Monopicolinate Cross-Bridged Cyclam Combining Very Fast Complexation with Very High Stability and Inertness of Its Copper(II) Complex

Luís M. P. Lima, Zakaria Halime, Ronan Marion, Nathalie Camus, Rita Delgado,* Carlos Platas-Iglesias, and Raphaël Tripier*

A two-step, easy to run synthesis and copper(II) complexation study of H**cb-te1pa**, a cross-bridged cyclam bearing one picolinate arm, are presented. The copper(II) complex shows an unusual, very fast complexation process, even in acidic medium, which is combined with its important thermodynamic stability and kinetic inertness.

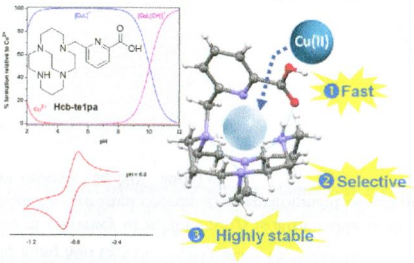

5280 Ⓢ dx.doi.org/10.1021/ic500510s

Acid–Base Chemistry in the Formation of Mackay-Type Icosahedral Clusters: μ_3-Acidity Analysis of Sc-Rich Phases of the Sc–Ir System

Yiming Guo, Timothy E. Stacey, and Daniel C. Fredrickson*

Using the μ_3-acidity model, we investigate of one most intriguing structural entities in intermetallics: the Mackay cluster of icosahedral quasicrystals. Analyses for a series of Sc–Ir intermetallics, including the Mackay cluster-based $Sc_{57}Ir_{13}$ and $Sc_{44}Ir_7$, reveal that each phase is stabilized by substantial μ_3-neutralization. Key to this result is the intergrowth of simple and tetrahedral close-packed arrangements, which maximizes neutralization of the acidic Sc by the basic Ir while minimizing the buffering role of Sc–Sc interactions.

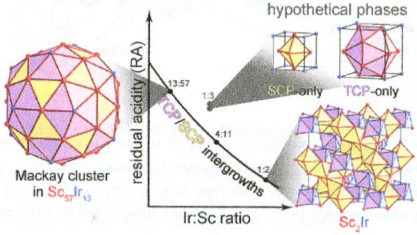

5294 S dx.doi.org/10.1021/ic500523a

Further Evidence for the Stabilization of U(V) within a Tetraoxo Core

Jared T. Stritzinger, Evgeny V. Alekseev,* Matthew J. Polinski, Justin N. Cross, Teresa M. Eaton, and Thomas E. Albrecht-Schmitt*

Through the use of supercritical water, two new complex uranyl borates were synthesized. One of these materials is the first $U^{V/VI}$ mixed-valent uranium borate.

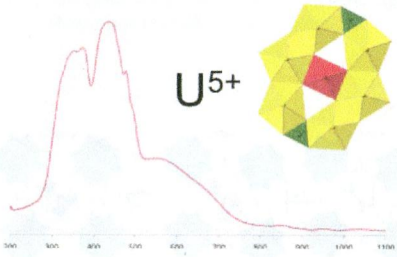

5300 S dx.doi.org/10.1021/ic5005243

Construction of the Tetrahedral Trifluorophosphine Platinum Cluster $Pt_4(PF_3)_8$ from Smaller Building Blocks

Peigang Hu, Qiong Luo,* Qian-shu Li, Yaoming Xie, R. Bruce King,* and Henry F. Schaefer

The experimentally known but structurally uncharacterized $Pt_4(PF_3)_8$ is predicted to be a distorted Pt_4 tetrahedron with four short Pt=Pt distances, two long Pt–Pt distances, and all terminal PF_3 groups. Theoretical thermochemical studies on the lower-nuclearity $Pt(PF_3)_n$ (n = 4, 3, 2), $Pt_2(PF_3)_n$ (n = 7, 6, 5, 4), and $Pt_3(PF_3)_6$ suggest the tetramerization of $Pt(PF_3)_2$ to $Pt_4(PF_3)_8$ to be highly exothermic regardless of the mechanistic details.

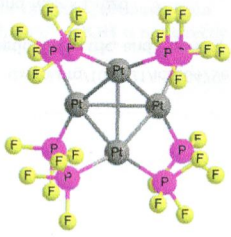

5311 S dx.doi.org/10.1021/ic500586g

A Tetranitrosyl [4Fe–4S] Cluster Forms En Route to Roussin's Black Anion: Nitric Oxide Reactivity of $[Fe_4S_4(LS_3)L']^{2-}$

Eric Victor and Stephen J. Lippard*

Previous studies provide evidence that [4Fe–4S] clusters serve as targets of reactive nitrogen oxide species in biology. The products of this reaction range from dinitrosyliron complexes, $[Fe(NO)_2L_2]^-$, to Roussin's black anion, $[Fe_4S_3(NO)_7]^-$. In this study, we prepared the site-differentiated complexes $[Fe_4S_4(LS_3)L']^{2-}$ to serve as synthetic models for biological [4Fe–4S] clusters and studied their reactivity toward NO(g) and Ph_3CSNO. The products were characterized by X-ray crystallography, mass spectrometry, and IR, electron paramagnetic resonance, and ^1H NMR spectroscopy.

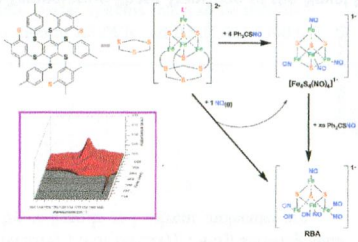

5321 Ⓢ dx.doi.org/10.1021/ic5006117

Stabilizing Radical Cation and Dication of a Tetrathiafulvalene Derivative by a Weakly Coordinating Anion

Feng Gao, Fei-Fei Zhu, Xing-Yong Wang, Yan Xu, Xin-Ping Wang,* and Jing-Lin Zuo*

The radical cation TMT-TTF$^{\bullet+}$ ($\mathbf{1}^{\bullet+}$) and dication TMT-TTF^{2+} ($\mathbf{1}^{2+}$) were successfully stabilized and isolated by the chemical oxidation of the neutral tetrakis(methylthio)tetrathiafulvalene (TMT-TTF, **1**) with specific oxidation agents, including weakly coordinating anion, $[Al(OR_F)_4]^-$ [OR_F = $OC(CF_3)_3$]. Both TMT-TTF$^{\bullet+}$ and TMT-TTF^{2+} are well-soluble in common organic solvents, as evidenced by UV−vis−NIR, ^{1}H NMR, and EPR studies in solution. The synthetic method is useful for new interesting charge transfer multifunctional molecular materials.

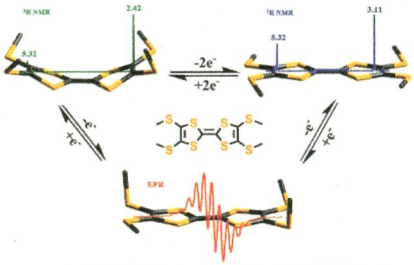

5328 Ⓢ dx.doi.org/10.1021/ic500636m

1,2-Addition of Dihydrogen across Rhodium(III)−OMe Bonds

Samantha A. Burgess, Deepa Devarajan, Tamara Bolaño, Daniel H. Ess,* T. Brent Gunnoe,* Michal Sabat, and William H. Myers

The net 1,2-addition of the H−H bond of dihydrogen across the Rh^{III}−OMe bond of $[(^t$bpy$)_2$Rh(OMe)(L)$][X]_n$ (^{t}bpy = 4,4′-di-*tert*-butyl-2,2′-bipyridyl; L = MeOH, *n* = 2, X = OTf (OTf = trifluoromethanesulfonate), TFA (TFA = trifluoroacetate); L = TFA, *n* = 1, X = OTf) is reported.

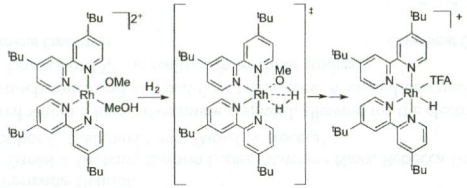

5341 Ⓢ dx.doi.org/10.1021/ic500642v

Amphiprotic Properties of a Bis(μ-hydroxo)divanadium(IV)-Substituted γ-Keggin-Type Silicodecatungstate Containing Two Different Kinds of Hydroxyl Moieties

Kazuhiro Uehara, Takuya Miyachi, and Noritaka Mizuno*

A bis(μ-hydroxo)divanadium(IV)-substituted γ-Keggin-type silicodecatungstate, $(TBA)_4[\gamma\text{-}SiV^{IV}_2W_{10}O_{36}(\mu\text{-}OH)_4]$ (**1**), possesses two different kinds of hydroxyl groups and can work as an amphiprotic species to accept and donate proton(s). The hydroxyl groups between tungsten atoms exhibit Brønsted acid properties, whereas the hydroxyl groups between two vanadium centers exhibit basic properties. The isoelectronic substitution of "V^{5+}" in $(TBA)_4[\gamma\text{-}SiV^{V}_2W_{10}O_{38}(\mu\text{-}OH)_2]$ with "V^{4+} + H^+" produced the more acidic protons at oxygen atoms between two tungsten atoms.

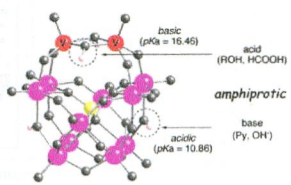

5348 S

dx.doi.org/10.1021/ic500684b

Synthesis, Structural Characterization, and Reactivity Studies of 5-CF_3SO_3-$B_{10}H_{13}$

Emily R. Berkeley, William C. Ewing, Patrick J. Carroll, and Larry G. Sneddon*

The reaction of *closo*-$B_{10}H_{10}^{2-}$ with triflic acid at 60 °C in ionic liquid solution results in cage opening to produce the triflate-functionalized decaborane 5-TfO-$B_{10}H_{13}$ (TfO = CF_3SO_3). Reactivity studies demonstrate that 5-TfO-$B_{10}H_{13}$ and its derivatives can be converted to a range of useful polyboranes and carboranes.

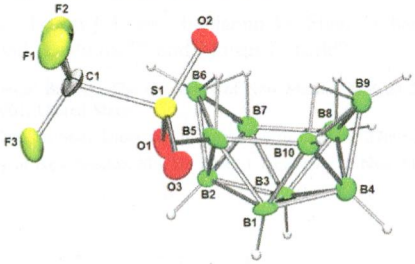

5359 S

dx.doi.org/10.1021/ic500723y

Prototypical Phosphine Complexes of Antimony(III)

Saurabh S. Chitnis, Neil Burford,* Robert McDonald, and Michael J. Ferguson

Chloroantimony complexes with phosphine ligands featuring a variety of coordination geometries and charges have been prepared and comprehensively characterized. The observed structural outcomes are rationalized using a *trans* influence series. ^{31}P NMR spectroscopy is shown to be a sensitive probe of the electronic environment at the antimony center. The structure and bonding in these complex are investigated using density functional theory calculations.

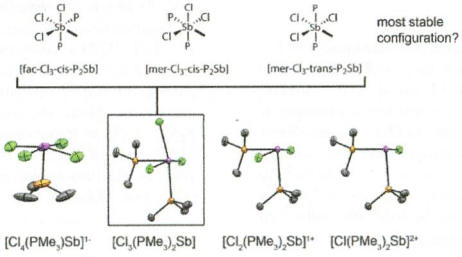

5373 Ⓢ dx.doi.org/10.1021/ic500777d

Direct Probing of Photoinduced Electron Transfer in a Self-Assembled Biomimetic [2Fe2S]-Hydrogenase Complex Using Ultrafast Vibrational Spectroscopy

Ping Li, Saeed Amirjalayer, František Hartl,* Martin Lutz, Bas de Bruin, René Becker, Sander Woutersen,* and Joost N. H. Reek*

Photoinduced electron transfer in a supramolecular ZnTPP·Fe_2S_2 complex is investigated using femtosecond infrared spectroscopy, infrared spectro-electrochemistry, and DFT calculations. We find that the electron density is delocalized over the diiron core and the naphthalimide ligand, which explains the photocatalytic properties of this complex. The results show that time-resolved infrared spectroscopy provides a unique tool to investigate photoinduced electron transfer in Fe_2S_2·porphyrin systems, and so to optimize their performance for the production of solar fuels.

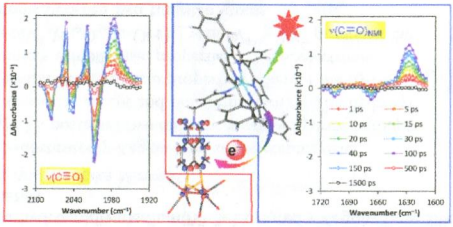

5384 Ⓢ dx.doi.org/10.1021/ic500759g

Electron-Transfer Studies of a Peroxide Dianion

Andrew M. Ullman, Xianru Sun, Daniel J. Graham, Nazario Lopez, Matthew Nava, Rebecca De Las Cuevas, Peter Müller, Elena V. Rybak-Akimova, Christopher C. Cummins,* and Daniel G. Nocera*

A peroxide dianion can be isolated within a hexacarboxamide cryptand, allowing for the electron-transfer (ET) kinetics of this species to be studied using electrochemical and stopped-flow techniques. A unified description of the heterogeneous and homogeneous outer-sphere ET kinetics of O_2^{2-} is realized from these studies.

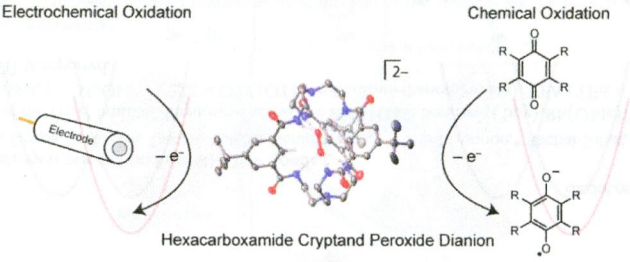

5392 Ⓢ dx.doi.org/10.1021/ic500914j

Copper Phenanthrene Oxidative Chemical Nucleases

Zara Molphy, Andreea Prisecaru, Creina Slator, Niall Barron, Malachy McCann, John Colleran, Deepak Chandran, Nicholas Gathergood, and Andrew Kellett*

A series of copper(II) phenazine−phenanthroline complexes are reported, and their interaction with ctDNA, poly[d(A-T)$_2$], and poly[d(G-C)$_2$] reveal DPQ, DPPZ, and DPPN compounds having superior binding constants (10^7 M(bp)$^{-1}$) and CpG-targeting properties compared to the well-studied chemical nuclease [Cu(1,10-phen)$_2$]$^{2+}$. Oxidative nuclease activity is identified using a novel microfluidic "on-chip" protocol developed for the Bioanalyzer 2100 platform with activity related to catalytic interactions with the superoxide anion and Fenton-type breakdown of hydrogen peroxide.

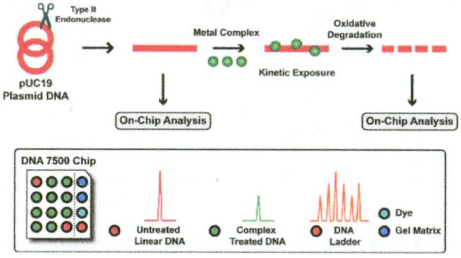

Ⓢ Supporting Information available via online article